Decomposed Phase Analysis for DER Hosting Capacity in Unbalanced Distribution Feeders

Hani Mavalizadeh and Mads R. Almassalkhi
Department of Electrical and Biomedical Engineering
University of Vermont
Burlington, USA
{hmavaliz, malmassa}@uvm.edu

***Abstract*—This paper uses convex inner approximations (CIA) of the AC power flow to tackle the optimization problem of quantifying a 3-phase distribution feeder's capacity to host distributed energy resources (DERs). This is often connoted hosting capacity (HC), but herein we consider separative bounds for each node on positive and negative DER injections, which ensures that injections within these nodal limits satisfy feeder voltage and current limits and across nodes sum up to the feeder HC. The methodology decomposes a 3-phase feeder into separate phases and applies CIA-based techniques to each phase. An analysis is developed to determine the technical condition under which this per-phase approach can still satisfy network constraints. New approaches are then presented that modify the per-phase optimization problems to overcome conservativeness inherent to CIA methods and increase overall HC, including selectively modifying the per-phase impedances and iteratively relaxing per-phase voltage bounds. Discussion is included on trade-offs and feasibility. To validate the methodology, simulation-based analysis is conducted with the IEEE 37-node test feeder and a real 534-node unbalanced radial distribution feeder.**

***Index Terms*—Distributed energy resources, convex optimization, hosting capacity, distribution system, 3-phase power.**

NOMENCLATURE

Sets and Indices

$\mathcal{E}$	Set of edges (branches) in the distribution feeder
$\mathcal{V}$	Set of nodes in the distribution feeder
G	Graph representing the distribution feeder
i, j	Indices representing nodes in the distribution feeder

Parameters and Constants

α	Coefficient for adjusting voltage bounds based on voltage deviation
N	Total number of nodes in the distribution feeder
r_{ij}	Resistance component of branch impedance between nodes i and j
V_0	Fixed voltage at the substation (slack) node
x_{ij}	Reactance component of branch impedance between nodes i and j
z_{ij}	Branch impedance between nodes i and j
$Z_{ij}^{3\phi}$	Impedance matrix for a 3-phase line section between nodes i and j
$\overline{V}$	Vector of lower limits on node voltages
$\underline{V}$	Vector of upper limits on node voltages
C	Incidence matrix of the feeder graph
R, X	Diagonal matrices of resistance and reactance components
W	Diagonal matrix of squared branch impedances

Variables

$\Delta V_{ij}^{3\phi}$	Voltage drop vector between nodes i and j
ΔW_i	Voltage margin at bus i
E_i^l	Determines how much the voltage has exceeded the lower limit at node i
E_i^u	Determines how much the voltage has exceeded the upper limit at node i
$I_{ij}^{3\phi}$	Current vector in branch (i, j) for a 3-phase system
$I_{ij}^{3\phi}$	Current vector in branch (i, j)
l_{ij}	Square of the current phasor in branch (i, j)
M_v	Maximum violation per unit
N_v	Total number of violations
p_i	Active power injection at node i
P_{ij}, Q_{ij}	Active and reactive power flows in branch (i, j)
q_i	Reactive power injection at node i
s_i	Complex power injection at node i
S_V	Sum of violations, captures the cumulative severity of violations across the network
V_i	Square of the voltage phasor magnitude at node i
V_i^{est}	Estimated voltage in the IVB at node i
V_i^{per}	Voltage from per-phase optimization in the IVB at node i
$V_i^{3\phi}$	Voltage vector at 3-phase node i
W_M	Average voltage margin
l	Vector of squared current phasor magnitudes in all branches
P, Q	Vectors of active and reactive power flows in all branches
P^+, Q^+, l^+	Upper proxy variables for active, reactive power and squared current.
P^-, Q^-, l^-	Lower proxy variables for active, reactive power and squared current.
HC	Hosting Capacity

The authors graciously recognize support from the National Science Foundation (NSF) Award ECCS-2047306. This material is also based upon work supported by the U.S. Department of Energy's Office of Energy Efficiency and Renewable Energy (EERE) under the Solar Energy Technologies Office Award Number DE-EE0010147. The views expressed herein do not necessarily represent the views of the U.S.Department of Energy or the United States Government.

$P_{\text{HC}}^{3\phi}$ 3-phase Hosting Capacity
VUF Voltage Unbalance Factor

I. Introduction

As the deployment of distributed energy resources (DERs) in power grids continues to accelerate, their utilization in a number of ancillary services is increasing [1]. In this context, DERs can be managed by aggregators, which dispatch them in response to market signals, often without taking into account the limitations of the grid. This lack of consideration can potentially lead to violations of critical grid constraints, including voltage and transformer limits. Therefore, there is an urgent need for what is referred to as *Grid-aware DER coordination*, which involves effectively accounting for AC network constraints during the coordination of DERs [2].

Various methods have been proposed in the technical literature for grid-aware DER coordination. One common approach is to restrict the amount of power that each customer can export to the grid [3]. However, this method can be overly conservative, and with the rapid increase in the number of DERs connected to the grid, these fixed limits can become outdated and require frequent updates [4].

In direct control schemes, it is assumed that the grid operator has access to all DER data and can directly control DERs [5], [6]. While direct control methods can theoretically provide optimal solutions, they often rely on strong assumptions related to observability and controllability. In practice, DER aggregators do not have access to grid data, and grid operators do not have full control over DERs.

Alternatively, [7] proposes an approach where the grid operator adjusts locational marginal prices (LMPs) based on grid conditions to incentivize the aggregator to adapt the DER aggregate load accordingly. However, this paper assumes a balanced distribution system, which may not hold in real-world applications. In [8], two mechanisms are presented to allow the grid operator to override DER aggregator dispatch decisions to ensure grid constraints are not violated. One limitation is that in certain electric markets, the grid operator may not have the authority to block aggregator control decisions.

Another approach is for the grid operator to establish limits on the amount of injection from each node to preserve grid constraints. This approach requires minimal information exchange between the grid operator and aggregator. In [4], the concept of *operating envelopes* is introduced, where the grid operator uses linear or model-free methods to issue time-varying export/import limits to aggregators. A convex inner approximation (CIA) is presented in [9] for maximizing voltage margins, which is generalized in [10] to compute feeder hosing capacity of balanced or single-phase distribution feeders. In [11], a sequential algorithm is presented that constructs a convex restriction around an initial feasible point, subsequently refining it to obtain an improved feasible solution. This work is extended further in [12], where the approach is enhanced to account for robustness against uncertainty in power injections. In [13], a model-free approach is introduced, leveraging historical meter data and neural networks to eliminate the need for solving the non-convex AC OPF problem in unbalanced distribution feeders. It demands access to substantial volumes of meter data, which may not always be readily available. Additionally, it's important to note that model-free methods can exhibit sensitivity to the quality and distribution of data. In [14] a bottom-up approach is presented where DERs submit power injection requests based on their local controllers to the grid operator. The grid operator can deny injection requests if a 3-phase power flow analysis indicates a risk of grid constraint violation. An optimization model for assessing the hosting capacity (HC) of DERs, taking into consideration the anticipated network conditions during demand response scheduling and adapting to the real-time network state is developed in [15].

Thus, in the literature, there are either simplified models used to compute hosting capacities with no guarantees or guarantees applicable only to simplified systems. It is within this context that this paper contributes to the field of computing hosting capacity for realistic systems with outlined trade-offs between optimality and guaranteed feasibility:

- The recently presented optimization-based approach for computing the (dynamic) hosting capacity of single-phase distribution feeders in [10] has been extended to 3-phase, unbalanced distribution feeders. This extension is further adapted to account for mutual impedances in the original optimization problem.
- The HC estimate for unbalanced feeders is then improved by iteratively adjusting voltage bounds within the per-phase optimization framework, accounting for mutual impedances and unbalanced load in the 3-phase system.
- Finally, the methodology is validated through simulation-based analysis on the IEEE 37-node feeder and a real 3-phase network with more than 500 3-phase nodes.

The remainder of the paper is organized as follows: Section II provides a concise overview of the power flow equations for single-phase and 3-phase radial distribution feeders.The CIA-based method to obtain HC for balanced distribution feeders is detailed in Section III, while the proposed approach to extend the method to 3-phase unbalanced grids is presented in Section IV. Finally, numerical results are provided in Section V followed by concluding remarks in Section VI.

II. Distribution Power Flow

A. Single-Phase Power Flow

Consider a radial (single-phase) distribution feeder as a tree graph $G = (\mathcal{V}, \mathcal{E})$ with N nodes $\mathcal{V} := \{1, \ldots, N\}$ and $N-1$ branches $\mathcal{E} \subseteq \mathcal{V} \times \mathcal{V}$, such that if nodes i and j are connected, then $(i, j) \in \mathcal{E}$. At each node $i \in \mathcal{V}$, consider the square of the voltage phasor magnitude, i.e., $v_i := |V_i|^2$ and the complex power injections, which are denoted $s_i = p_i + \mathbf{j}q_i$. Node 0 is assumed to be the substation (slack) node with a fixed voltage $v_0 = |V_0|^2$. For each branch with impedance $z_{ij} = r_{ij} + \mathbf{j}x_{ij}$, we consider the square of the current phasor, i.e., $l_{ij} := |I_{ij}|^2$ and the active and reactive power flows, P_{ij} and Q_{ij}. In a balanced, radial distribution feeder, the

relations between v_i, l_{ij}, active/reactive power flows P_{ij}/Q_{ij}, and net active/reactive injections p_i/q_i can be expressed by the nonlinear *DistFlow* model [16]:

$$v_i = v_j + 2r_{ij}P_{ij} + 2x_{ij}Q_{ij} - |z_{ij}|^2 l_{ij}, \quad \forall (i,j) \in \mathcal{E} \tag{1a}$$

$$P_{ij} = p_i + \sum_{h:(h,i)\in\mathcal{E}} (P_{hi} - r_{hi}l_{hi}), \quad \forall (i,j) \in \mathcal{E} \tag{1b}$$

$$Q_{ij} = q_i + \sum_{h:(h,i)\in\mathcal{E}} (Q_{hi} - x_{hi}l_{hi}), \quad \forall (i,j) \in \mathcal{E} \tag{1c}$$

$$l_{ij}v_i = P_{ij}^2 + Q_{ij}^2, \quad \forall (i,j) \in \mathcal{E}, \tag{1d}$$

where the nonlinearity arises from (1d). Before addressing the nonlinearity, consider the three linear expressions in (1), for which we develop the linear matrix equations that directly relate net injections to P, Q, and V. By using the incidence matrix B of the radial network and applying [17], the power flows can be expressed as a linear functions of the net power injections and the branch currents as:

$$P = Cp - D_R l, \quad Q = Cq - D_X l, \tag{2}$$

where, $C = (I_N - A)^{-1}$, $D_R = CAR$, and $D_X = CAX$, $P = [P_{ij}]_{(i,j)\in\mathcal{E}}, Q = [Q_{ij}]_{(i,j)\in\mathcal{E}}, p = [p_i]_{i\in\mathcal{V}}, q = [q_i]_{i\in\mathcal{V}}, R = \text{diag}\{r_{ij}\}_{(i,j)\in\mathcal{E}}, X = \text{diag}\{x_{ij}\}_{(i,j)\in\mathcal{E}}, l = [l_{ij}]_{(i,j)\in\mathcal{E}}$. and $A = [0_N \quad I_N]B - I_N$, where I_N is the $N \times N$ identity matrix and 0_N is a column vector of n rows. By recursively applying (1a), the following voltage relations can be obtained,

$$[v_i - v_j]_{(i,j)\in\mathcal{E}} = 2(RP + XQ) - Wl, \tag{3}$$

where $W := \text{diag}\{|z_{ij}|^2\}_{(i,j)\in\mathcal{E}}$. The left hand side of (3) can be written as a function of slack node,

$$C^\top [v_i - v_j]_{(i,j)\in\mathcal{E}} = V - v_0 1_n, \tag{4}$$

where $V := [v_i]_{i\in\mathcal{V}}$. By combining (3) and (4) we get

$$V = v_0 1_n + 2(C^\top RP + C^\top XQ) - C^\top Wl. \tag{5}$$

Finally, by substituting (2) in (5), the relation between voltages and power injections becomes

$$V = v_0 1_n + M_P p + M_Q q - Hl, \tag{6}$$

where $M_P = 2C^\top TRC$, $M_Q = 2C^\top XC$, and $H = C^\top(2(D_R + XD_X) + W)$. The compact representation of P and Q in (2) and V in (6) is equivalent to the scalar form of their respective DistFlow equations in (1). Clearly, if we can eliminate or simplify expression of l in (1d), we would have a linear or convex representation of the *DistFlow* model. Since we are interested in hosting capacity, we desire a predictive model, where all *feasible* net injections result in voltages and branch flows within limits. To achieve this, we leverage a convex envelope on (1d) to construct a convex inner approximation that over- and under-estimates l (resp. l^+ and l^-) and use these appropriately to construct over- and under approximations of P, Q, V (resp. $[P^+, Q^+, V^+]$ and $[P^-, Q^-, V^-]$) and subject these to their respective limits, e.g., $\underline{V} \le V^-$ and $V^+ \le \overline{V}$. This process is outlined in the Appendix.

Since this paper focuses on adapting the convex inner approximation of the (balanced) *DistFlow* model to realistic 3-phase feeders, the next subsection will briefly describe 3-phase distribution power flows and introduce the 3-phase notation.

B. 3-phase distribution power flow

Consider a 3-phase, radial graph G, wherein each node represents three phases: a, b, c. Similarly, each branch represents a 3-phase line section with a corresponding 3×3 impedance matrix, which is expressed as,

$$z_{ij}^{3\phi} := \begin{bmatrix} z_{ij}^{\text{a}} & z_{ij}^{\text{ab}} & z_{ij}^{\text{ac}} \\ z_{ij}^{\text{ba}} & z_{ij}^{\text{b}} & z_{ij}^{\text{bc}} \\ z_{ij}^{\text{ca}} & z_{ij}^{\text{cb}} & z_{ij}^{\text{c}} \end{bmatrix} \forall (i,j) \in \mathcal{E}. \tag{7}$$

Voltage at 3-phase node i is denoted $V_i^{3\phi} = \left[V_i^a, V_i^b, V_i^c\right]^\top$ and current in branch $(i,j) \in \mathcal{E}$ is $I_{ij}^{3\phi} = \left[I_{ij}^a, I_{ij}^b, I_{ij}^c\right]^\top$. The line voltage drop and currents are related by

$$\Delta V_{ij}^{3\phi} := V_i^{3\phi} - V_j^{3\phi} = z_{ij}^{3\phi} I_{ij}^{3\phi} \Rightarrow \Delta V^{3\phi} = Z^{3\phi} I^{3\phi}, \tag{8}$$

where, $I^{3\phi} = [I_{ij}^{3\phi}]_{(i,j)\in\mathcal{E}} \in \mathbb{C}^{3(N-1)}$ represents the complex 3-phase currents, $V^{3\phi} = [V_i^{3\phi}]_{i\in\mathcal{V}} \in \mathbb{C}^{3N}$ corresponds to the 3-phase voltages, $Z^{3\phi} \in \mathbb{C}^{3(N-1)\times 3(N-1)}$ is the complex 3-phase impedance matrix.

III. Balanced feeder HC via CIA

This section describes the modeling of distribution feeders and their hosting capacity (HC). The CIA-based approach detailed in [9], [10] employs a CIA of the set of feasible admissible injections. An optimization problem is used to determine the HC at each node of a distribution feeder. The total feeder HC is the sum across all nodes.

The non-linear (1d) makes the *DistFlow* formulation non-convex within an optimal power flow (OPF) problem. Thus, we are interested in utilizing a CIA of the *DistFlow*. The CIA effectively bounds the nonlinear l_{ij} with a convex envelope: $l_{ij}^-(P,Q,V) \le l_{ij}(P,Q,V) \le l_{ij}^+(P,Q,V)$, which enables the creation of two sets of variables: upper ($^+$) and lower proxies ($^-$), e.g., $V^- \le V \le V^+$. As long as the lower proxies satisfy lower limits and upper proxies satisfy upper limits, e.g., $\underline{V} \le V^-$ and $V^+ \le \bar{V}$, then we are guaranteed that the physical variable satisfies, e.g., $\underline{V} \le V \le \bar{V}$. This guarantee means that we can replace the physical variables altogether and replace them with their convex proxies.

In this paper, we consider feeders with inductive branches[1], i.e., $x_{ij} \ge 0$, $\forall (i,j) \in \mathcal{E}$. In this case, the elements of the

[1]Note that while models and methods presented herein make use of inductive networks, their extension to distribution feeders with arbitrary impedances is straightforward.

H matrix are non-negative [9]. Then, we can replace the non-convex formulation in (1d) and (6) with their convex proxies:

$$V^+ = V_0\mathbf{1}_N + M_p p + M_q q - Hl^-, \tag{9a}$$
$$V^- = V_0\mathbf{1}_N + M_p p + M_q q - Hl^+, \tag{9b}$$
$$P^+ = Cp - D_R l^-, \tag{9c}$$
$$P^- = Cp - D_R l^+, \tag{9d}$$
$$Q^+ = Cq - D_X l^-, \tag{9e}$$
$$Q^- = Cq - D_X l^+. \tag{9f}$$
$$l^+ \geq f_{\text{quad}}(P^+, P^-, Q^+, Q^-, V^+, V^-) \tag{9g}$$
$$l^- := f_{\text{aff}}(P^+, P^-, Q^+, Q^-, V^+, V^-), \tag{9h}$$

where l^- is affine in the proxy variables while l^+ is a convex relaxation of a quadratic function of the proxy variables. Please see Appendix A for derivations of f_{aff} and f_{quad} and [9], [10] for full details. Finally, the feeder HC is then the maximum sum of nodal injections, $p_i^+ := p_i^*$, that drives the feeder to its capacity (e.g., voltage, current, or power flow limits are active). The convex formulation that achieves this objective is

$$\mathbf{P}_{\text{CIA}}^{\phi,+}: \quad p^+ := \arg\max_{p_i} \sum_{i=1}^{N} w_i p_i, \tag{10a}$$
$$\text{subject to (9)} \tag{10b}$$
$$\underline{l} \leq l^-, \tag{10c}$$
$$l^+ \leq \bar{l}, \tag{10d}$$
$$\underline{V} \leq V^-, \tag{10e}$$
$$V^+ \leq \overline{V}, \tag{10f}$$
$$p_i^2 + q_i^2 \leq \overline{s_i}^2, \quad \forall i \in \mathcal{V}, \tag{10g}$$

where w_i are design parameters that differentiate nodal capacities. Note that inequality (10g) is optional and captures limits on active injections based on apparent power limits at each node (e.g., from inverter, transformer, or power factor limits). Other constraints on $P^{+/-}, Q^{+/-}$ may also be added.

The HC for DER injections (e.g., solar PV) is defined as

$$\overline{\text{HC}} := \sum_{i}^{N} p_i^+ = \mathbf{1}_N^\top p^+ > 0. \tag{11}$$

Similarly, we can define the HC relative to consumption (e.g., electric vehicle HC) as $\underline{\text{HC}} := \sum_i^N p_i^- = \mathbf{1}_N^\top p^- < 0$, where p^- is the solution that minimizes the nodal (net) injections, i.e., solve corresponding $\mathbf{P}_{\text{CIA}}^{\phi,-}$ problem, whose details are omitted due to page limits. Thus, $\underline{\text{HC}} \leq 0 \leq \overline{\text{HC}}$.

However, since $\mathbf{P}_{\text{CIA}}^{\phi,+}$ and $\mathbf{P}_{\text{CIA}}^{\phi,-}$ employ a CIA of *DistFlow*, the HC estimates are valid only for balanced, radial distribution feeders. We are now interested in how to adapt this CIA-based method to a realistic unbalanced distribution feeder, which means that we need to consider the effects of mutual phase impedance and load unbalances.

Next, we seek to extend the CIA-based method from balanced (single-phase equivalent) feeders to unbalanced feeders.

IV. Unbalanced Feeder HC via CIA

Given an unbalanced feeder, how can we approximate or decompose it for HC analysis? In this section, we seek to answer this question.

A. Extending CIA to unbalanced feeders

In this subsection we specifically consider methods for 1) approximating feeders as balanced (e.g., by modifying line impedances and nodal loads and 2) decomposing feeders along their phases. These are summarized next.

- **Method 1 - balanced feeder approximation:** This strategy involves transforming an unbalanced feeder into an *approximate* balanced model, which is then used to determine p^-, p^+ from $\mathbf{P}_{\text{CIA}}^{\phi,+\backslash-}$. The resulting per-phase HC is then distributed equally to each phase. We consider two different ways to approximate a balanced feeder:
  - i) Take the maximum line impedance and minimum loads across all three phases to capture the worst-case voltage drop/rise.
  - ii) Average line impedances and loads across phases a/b/c to create a balanced approximation of a feeder. This approximation can potentially cause voltage violations at the corresponding HC value.
- **Method 2 - per-phase analysis:** In this approach, we extract each phase separately and compute p^- and p^+. This per-phase approach is considered for two different implementations:
  - i) One phase is selected and nodal HC values, (p_i^-, p_i^+), are computed for that phase. For the 3-phase feeder, the same (p_i^-, p_i^+) values are then applied to all phases at a 3-phase node. We denote the sub-methods 2i$^\phi$ for $\phi = \{\text{a}, \text{b}, \text{c}\}$, e.g., $\overline{\text{HC}}_{3\phi} = 3 \times \mathbf{1}_N^\top p_{\text{a}}^+$ for method 2i^a.
  - ii) All three phases are extracted separately and we compute (p^-, p^+) for each phase, which yields hosting capacity, e.g., $\overline{\text{HC}}_{3\phi} = \mathbf{1}_N^\top (p_{\text{a}}^+ + p_{\text{b}}^+ + p_{\text{c}}^+)$.

Each of these methods estimates the 3-phase HC, e.g., $\overline{\text{HC}}$ by computing net nodal injections, e.g., p_ϕ^+, which are then applied to the full 3-phase network to determine the corresponding 3-phase voltages and currents. In Fig.1, these voltage and current profiles for Method 2ii are presented for the IEEE 37-node test feeder [18]. As can be seen, despite single-phase analysis underpinning the HC estimate, phase voltages are within $\overline{V} = 1.05$ pu across all nodes and phases. Next, we are interested in metrics that can be used to compare the different methods.

- **Total number of violations**, N_v, counts the number of nodes and phases for which $|V_i^{3\phi}| \notin [\underline{V}, \overline{V}]$.
- **Maximum violation in per unit**, M_v, provides a measure of the severity of the violations:

$$M_v = \max_{i=1,\ldots,3N} \left\{ \max\left\{0, E_i^{\text{u}}, E_i^{\text{l}}\right\} \right\}, \tag{12}$$

where, $E^{\text{u}} := |V^{3\phi}| - \overline{V}\mathbf{1}_{3N}$ and $E^{\text{l}} := \underline{V}\mathbf{1}_{3N} - |V^{3\phi}|$.

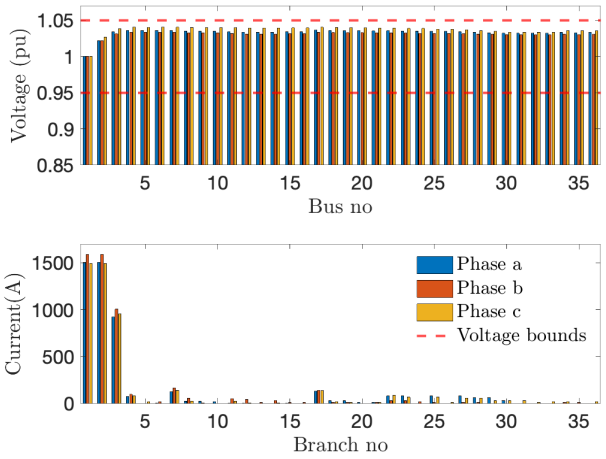

Fig. 1. Illustrating the effects of D3P on 3-phase voltage and current profiles following the addition of nodal injections $p_a^+ + p_b^+ + p_c^+$. The dashed red line indicates the ANSI voltage limits of [0.95, 1.05] pu.

- **Sum of violations**, S_v, captures the cumulative severity of violations across the network:

$$S_v = \sum_{i=1}^{3N} \max\left(0, E_i^{\mathrm{u}}, E_i^{\mathrm{l}}\right). \tag{13}$$

- **Average voltage margin**, W_M, measures how conservative the HC results from $\mathbf{P}_{\mathrm{CIA}}^{\phi,+/-}$ are:

$$W_M = \frac{1}{3N} \sum_{i=1}^{3N} \max\left\{0, \Delta W_i\right\}, \tag{14}$$

where $\Delta W_i := \min\left\{|V_i^{3\phi}| - \underline{V}, \overline{V} - |V_i^{3\phi}|\right\}$.

- **Voltage unbalance factor (VUF)** provides a relative measure (in %) of voltage unbalance caused by nodal HC injections:

$$\mathrm{VUF} = \frac{100}{N} \sum_{i=1}^{N} \frac{\max\left\{|V_i^{3\phi}| - \frac{1}{3}\mathbf{1}_3^\top |V_i^{3\phi}| \mathbf{1}_3\right\}}{\frac{1}{3}\mathbf{1}_3^\top |V_i^{3\phi}|}. \tag{15}$$

It should be noted that none of the methods leads to voltage violation in the IEEE 37 node feeder. That is due to the inherent conservativeness of the CIA. To compare Methods 1 and 2, we consider three scenarios: i) increase all loads in phase c by 20% and decrease all loads on phase b by 20%; ii) from scenario i, swap the loads of phases b and c; iii) from scenario i, swap loads of phases a and b. Throughout, the power factor is kept constant. Table I uses the metrics above to compare minimum HC estimates, i.e., using $\mathbf{P}_{\mathrm{CIA}}^{\phi,-}$, average of W_M and VUF, sum of S_v and N_v, across scenarios i, ii and iii. Notably, the comparison shows that Method 2ii does not cause voltage violations. Method 1i leads to an overly loaded network which makes the optimization problem infeasible. Other methods result in voltage violations. Thus, based on results in Table I, Method 2ii is selected for further analysis. In the remainder of this paper, this technique shall be referred

TABLE I
PERFORMANCE OF THE PROPOSED METHODS

Method	N_v	M_v(pu)	S_v (pu)	W_M (pu)	HC (MW)	VUF (%)
$1i$	0	0	0	0.039	N/A	0.81
$1ii$	17	0.005	0.040	0.017	-14.68	0.87
$2i^{\mathrm{a}}$	18	0.010	0.085	0.017	-14.03	0.88
$2i^{\mathrm{b}}$	33	0.013	0.158	0.017	-11.07	0.92
$2i^{\mathrm{c}}$	4	0.003	0.009	0.022	-10.03	0.81
$2ii$	0	0	0	0.019	-13.98	0.48

to as the Decomposed 3-phase (D3P) method. Given that the D3P uses information from all phases without averaging, it was somewhat expected that D3P could outperform the other approaches. It should be noted that considering the mutual impedance can lead to less or more conservative HC depending on the characteristics of z_{ij}^m. In the next subsection, technical conditions are presented under which per-phase analysis and HC optimization extend to 3-phase networks.

B. Accounting for mutual impedance

In this subsection, we present an approach for adapting the per-phase HC estimates to deal with the inherent conservativeness of CIA. The method effectively modifies the impedance matrix to take into account the impact of mutual impedance. The approach makes the following assumptions:

Assumption 1. *The sum of the phase load currents is zero.*

Assumption 2. *3-phase lines are transposed, such that mutual impedances are identical:* $z_{ij}^{3\phi} = \begin{bmatrix} z_{ij}^a & z_{ij}^m & z_{ij}^m \\ z_{ij}^m & z_{ij}^b & z_{ij}^m \\ z_{ij}^m & z_{ij}^m & z_{ij}^c \end{bmatrix}$.

From the above assumptions, the following theorem holds.

Theorem 1. *Given a 3-phase system that satisfies Assumptions 1 and 2, if per-phase optimization* $\mathbf{P}_{CIA}^{\phi,+}$ *satisfies* $\underline{V} \leq V_i(p^+) \leq \overline{V}\ \forall i \in \mathcal{V}$, *then the 3-phase system satisfies* $\underline{V} \leq V_i^{3\phi}(p^+) \leq \overline{V}\ \forall i \in \mathcal{V}$. *Same holds for* $\mathbf{P}_{CIA}^{\phi,-}$ *and* $V_i(p^-)$.

***Proof**: The proof proceeds directly by utilizing Assumptions 1 and 2, and symmetrical components method [19] along with the matrix representation of KVL equations.*

Theorem 1 states a 3-phase distribution feeder can be decomposed into three decoupled single-phase distribution systems with modified impedances, $z_{ij}^{\phi} - z_{\mathrm{ij}}^m$, to ensure that the resulting HC will be feasible, i.e., does not lead to voltage violations in the 3-phase system. In this approach the grid information, particularly mutual impedances, are utilized to adjust the impedances matrix of a predictive model used in the optimization problem to determine the HC.

Remark 1. *Using a similar approach, and by further assuming identical conductor impedances* $z_{ij}^a = z_{ij}^b = z_{ij}^c$, *Theorem 1 extends to Delta-connected loads.*

In practical settings, when Assumptions 1 and 2 do not hold, z_{ij}^m can be approximated by

$$z_{\text{ij}}^m \approx (z_{\text{ij}}^{\mathbf{ab}} + z_{\text{ij}}^{\mathbf{ac}} + z_{\text{ij}}^{\mathbf{bc}})/3. \tag{16}$$

From each phase, we construct a sub-feeder from which we can compute nodal HC (net) injections p_i^- and p_i^+ using D3P. The resulting voltages of the single-phase networks, $|V_i|$, are then compared with those of the full 3-phase load flow, $|V_i^{3\phi}|$, with the 3-phase (net) injections $p_{3\phi}^+ := [p_{a,i}^+, p_{b,i}^+, p_{c,i}^+]_{i\in\mathcal{V}}$ added to the system load. We denote the approach of solving $\mathbf{P}_{\text{CIA}}^{+/-}$ with modified impedance from Theorem 1 as **Mod-Z** HC.

In Fig. 2, a scatter plot of predicted single-phase and actual 3-phase voltage magnitudes is provided, i.e., $|V_i|$ vs. $|V_i^{3\phi}|$ for IEEE 37-node system, under D3P. The red dots represent $|V_i^{3\phi}|$ with additional injections $p_{3\phi}^+$ and the blue dots correspond to $|V_i^{3\phi}|$ when demands $p_{3\phi}^-$ added. Fig. 3 shows the results after applying **Mod-Z**. Specifically, in $\mathbf{P}_{\text{CIA}}^+$ and $\mathbf{P}_{\text{CIA}}^-$, the impedance of each line is augmented by the mutual impedance from (16). As expected, using Mod-Z, the single-phase voltages closely approximate the 3-phase voltages since (average) mutual impedances are considered explicitly. The small differences in Fig. 3 between $|V_i^{3\phi}|$ and $|V_i|$ are caused by the averaging error from z_{ij}^m in (16).

It should be noted that using the modified impedance in $\mathbf{P}_{\text{CIA}}^+$ and $\mathbf{P}_{\text{CIA}}^-$ successfully increases the HC by incorporating the mutual impedances in the $\mathbf{P}_{\text{CIA}}^+$ problem. Specifically, $\overline{\text{HC}}$ increases from 25.09 MW to 30.22 MW (a 20% increase), while $\underline{\text{HC}}$ increases from -14.89 MW to -19.30 MW (a 30% increase). However, this increase can lead to (minor) voltage excursions as seen in Fig. 3.

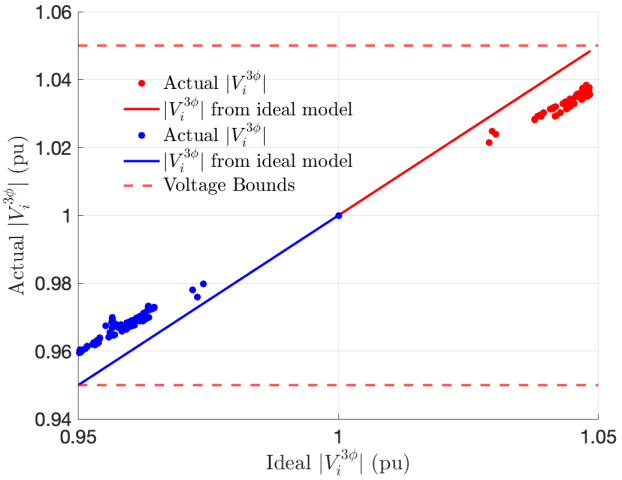

Fig. 2. Comparison of 3-phase voltages in the modified IEEE 37-node system, taking into account mutual impedances (actual) versus ignoring mutual impedances (ideal). In this figure, blue, and red correspond to voltages obtained using $\mathbf{P}_{\text{CIA}}^+$, and $\mathbf{P}_{\text{CIA}}^-$, respectively.

To mitigate these (minor) excursions, we present a heuristic approach that adjusts the impedance matrix in **Mod-Z**'s system model. Thus, instead of (coarsely) altering the impedance for

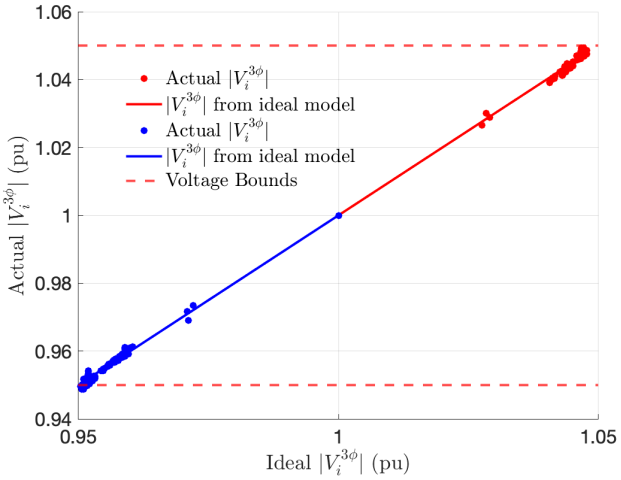

Fig. 3. Voltages magnitudes for the IEEE 37-node system after modifying the impedance matrix based on Mod-Z approach. In this figure, blue, and red correspond to voltages obtained using $\mathbf{P}_{\text{CIA}}^+$, and $\mathbf{P}_{\text{CIA}}^-$, respectively.

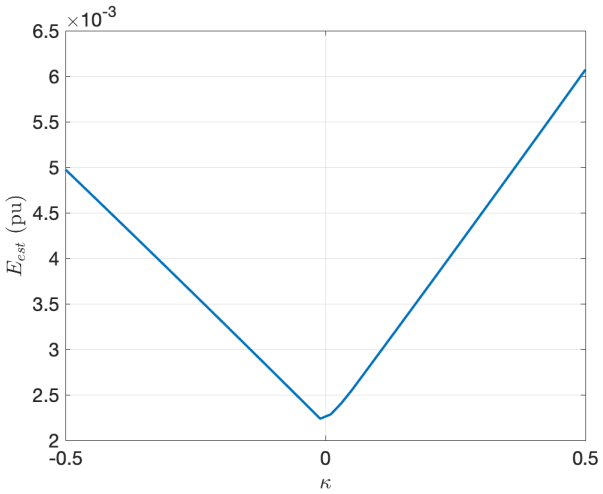

Fig. 4. Illustrating the impact of mutual impedance mismatch on the performance of **Mod-Z**.

all branches, only the impedances connected to a node i are modified, if the 3-phase simulated (i.e., predicted) voltage excursion exceeds a designated threshold ϵ, as follows:

$$\left||V_i^{3\phi}| - |V_i|\right| > \epsilon \quad \forall i. \tag{17}$$

We denote **Mod-Z**(ϵ) as the **Mod-Z** method with the chosen parameter ϵ. For example, $\epsilon = 0.0005$ means that voltage excursions smaller than 0.0005 pu are neglected and the impedances connected to those lines are not modified. Thus, decreasing $\epsilon \to 0$ leads to more lines being modified in **Mod-Z**(ϵ), which leads to higher predicted HC, but comes at the cost of more actual 3-phase voltage excursions. No free lunch in engineering.

To explore this tradeoff further, Table II presents the effects of different ϵ values in the **Mod-Z** approach. Clearly, with $\epsilon = 0.0010$ pu, only 9 of 36 lines are modified in $\mathbf{P}_{\text{CIA}}^+$, while

TABLE II
THE IMPACT OF MODIFYING THE IMPEDANCE MATRIX ON HC AND VOLTAGE VIOLATIONS FOR THE MODIFIED IEEE 37-NODE SYSTEM.

ϵ (pu)	0	0.0005	0.0010	D3P
$\overline{\text{HC}}$ (MW)	30.2	27.5	27.4	25.09
$\underline{\text{HC}}$ (MW)	-19.3	-17.5	-17.3	-14.9
N_v	10	5	0	0
M_v	0.0012	0.0004	0	0
# modified lines in $\mathbf{P}^{+}_{\text{CIA}}/\mathbf{P}^{-}_{\text{CIA}}$	36/36	22/27	9/16	0/0

all voltage violations are eliminated, and the reduction in HC is less than 10%. As ϵ increases fewer lines in the model will be modified. For a large enough ϵ, no lines will be modified, at which the **Mod-Z**(ϵ) results will match that of D3P.

We tested **Mod-Z** on two unbalanced networks, including IEEE 37-node test feeder and a realistic distribution feeder from Vermont. This allows us to study how unbalanced conditions in realistic networks affect the results. In both systems, the prediction error from optimizing single-phase Mod-Z formulation (under Equation (16) assumption) with the simulated reality of the unbalanced feeders was less than 0.002 pu across all nodes, all phases in either system. Notably, larger discrepancies in the mutual impedance across the three phases correlate with increased estimation errors, and vice versa.

To better illustrate the impact of mutual impedance discrepancies on estimation errors, a new experiment is introduced in the paper. In this experiment, the discrepancy in the given mutual impedance matrix is artificially increased by substituting z_{ij}^{ab} with $(1+\kappa)z_{ij}^{ab}$ and substituting z_{ij}^{bc} with $z_{ij}^{bc} - \kappa z_{ij}^{ab}$ for all lines and with $\kappa \in [-0.5, 0.5]$. These adjustments amplify the discrepancy in mutual impedance, i.e, makes the distribution system more unbalanced while keeping average z_{ij}^{m} constant. The scalar κ is systematically increased from -0.5 to 0.5, and at each increment, the estimation error, $E_{est} := |V_i^{3\phi} - V_i^{3\phi,ideal}|$, is computed to demonstrate the impact of differences in mutual impedances on the performance of **Mod-Z**, where $V_i^{3\phi,ideal}$ is the 3-phase voltages obtained by neglecting mutual impedances. The results are presented in Fig. 4.

This subsection showed the value of selectively modifying line impedances to enable per-phase optimization to apply directly to unbalanced distribution systems. Next, we seek to further enlarge the 3-phase HC by not just modifying impedances of each phase, but also by (incrementally) relaxing voltage bounds in the per-phase optimization formulation.

C. Iteratively modifying voltage limits

In this subsection, a novel approach, called iterative voltage bounds (IVB), is introduced that incrementally improves the 3-phase HC estimate by coupling 3-phase load flows with per-phase optimization $\mathbf{P}^{\phi,+\backslash-}_{\text{CIA}}$. The proposed method is summarized in Fig. 5 and outlined as follows for p^{+} $\overline{\text{HC}}$ (the approach is similar for p^{-} and $\underline{\text{HC}}$):

Step 1: *Single-phase optimization*: given per-phase voltage bounds $\underline{V}$ and $\overline{V}$, solve $\mathbf{P}^{+}_{\text{CIA}}$ for each phase using D3P to get nodal HC values p^{+}_{ϕ} and $\overline{\text{HC}}_{\phi}$.

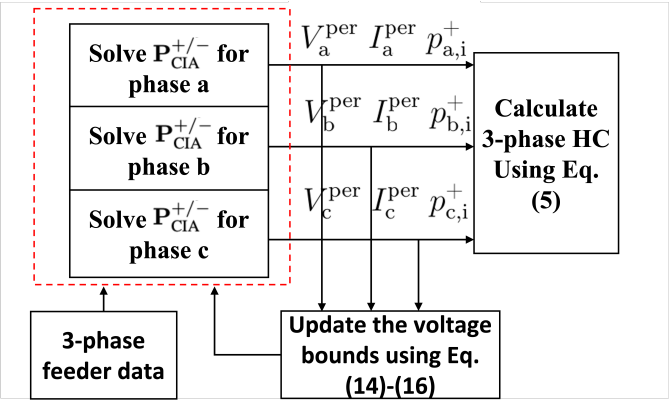

Fig. 5. Flowchart of the proposed IVB approach.

Step 2: *Single-phase load flow*: Apply p^{+}_{ϕ} to each phase ϕ and perform single-phase load flow: V_{ϕ}^{per} and I_{ϕ}^{per}.

Step 3: *3-phase load flow*: Apply $\{p^{+}_{\phi}\}_{\phi=\{a,b,c\}}$ to 3-phase system and perform load flow: $V^{3\phi}$ and $I^{3\phi}$.

Step 4: *Termination condition*: The algorithm stops if any element of $|V_i^{3\phi}|$ exceeds $[\underline{V}, \overline{V}]$.

Step 5: *Estimate per-phase voltage*: The per-phase model ignores mutual impedances, which leads to a voltage difference across phases relative to the 3-phase model. To estimate this difference, consider (8) and assume currents $I_{ij}^{\phi} \approx I_{ij,\phi}^{3\phi}$ are common across both the per-phase and 3-phase systems. Then, the estimated voltage for each phase becomes,

$$V_j^{\text{est}} = V_i^{\text{est}} - \begin{bmatrix} z_{ij}^{\text{a}} & z_{ij}^{\text{ab}} & z_{ij}^{\text{ac}} \\ z_{ij}^{\text{ba}} & z_{ij}^{\text{b}} & z_{ij}^{\text{bc}} \\ z_{ij}^{\text{ca}} & z_{ij}^{\text{cb}} & z_{ij}^{\text{c}} \end{bmatrix} I_{ij}^{3\phi} \quad \forall (i,j) \in \mathcal{E}. \tag{18}$$

Since v_0^{est}, i.e. head node voltage is known, the voltage of other nodes of a radial grid can be found using (18).

Step 6: *Per-phase voltage difference* : Using (18), the difference in per-phase voltage can be found as,

$$\Delta V_i = |V_i^{\text{est}}| - |V_i^{\text{per}}| \quad \forall i \in \mathcal{V}. \tag{19}$$

Step 7: *Updating voltage bounds*: the voltage bounds are updated for $\mathbf{P}^{\phi,+}_{\text{CIA}}$ to reflect the cumulative path voltage difference that arises due to per-phase optimization neglecting mutual impedances. The update is as follows:

$$\begin{aligned} \overline{V} &\leftarrow \overline{V} + \alpha \Delta V_i \\ \underline{V} &\leftarrow \underline{V} - \alpha \Delta V_i, \end{aligned} \tag{20}$$

where α is a design parameter that can be set to less than 1 to allow smaller steps in each iteration.

Step 8: *Iterate*: Go to **Step** 1.

We denote IVB(α) as the IVB method with the chosen parameter α. Next section, numerical results are presented to validate the proposed methodologies.

V. Numerical results

In this section, simulation results on the IEEE 37-node test system are presented together with a realistic 534-node radial distribution system from Vermont. IEEE 37-node test system is a 3-phase, unbalanced medium voltage (4.8 kV) network with a total load of 2.45 MW. The realistic feeder used in this paper is a 7.2 kV radial network including 534 nodes, 533 lines, and 160 loads with a total load of 2.47 MW. The MATLAB code provided by [20] is used for 3-phase simulations. Using the proposed approach enables an increase in the amount of HC without causing any additional violations. Fig. 6 shows the voltage bounds upon the termination of IVB. It can be seen that all of the 3-phase voltages are within $\underline{V}, \overline{V}$.

For the IEEE 37-node system, the results of p_i^- and p_i^+ obtained from different methods—D3P, Mod-Z(0.001), IVB(1) and IVB(0.1) are displayed in Fig. 7. Table III compares the simulation time and total HC for D3P, Mod-Z(0.001), and the IVB across two networks. It is worth noting that in the IVB, $\underline{\text{HC}}$ and $\overline{\text{HC}}$ consistently show improvements when utilizing the IVB. This enhancement is achieved by leveraging information regarding the mutual impedance of the grid. This increase in hosting capacity does not lead to any voltage violations, therefore no line modification is required in $\mathbf{P}_{\text{CIA}}^{\phi,+}$. That is, Mod-Z is not used with the IVB. In addition, observations indicate that while a decrease in α within the IVB framework leads to better outcomes, the computational burden escalates significantly. Thus, a compromise is necessary. Notably, reducing α does not enhance $\overline{HC}$, which can be contributed to the constraint being imposed by transformer capacity limits, rather than voltage constraints.

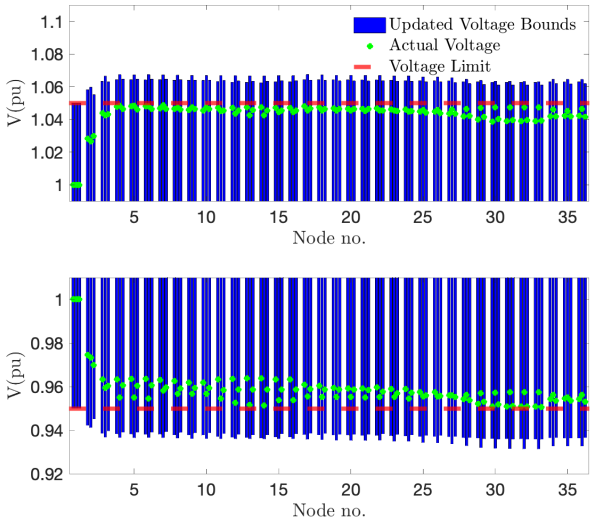

Fig. 6. Voltage bounds upon termination of the IVB(0.1).

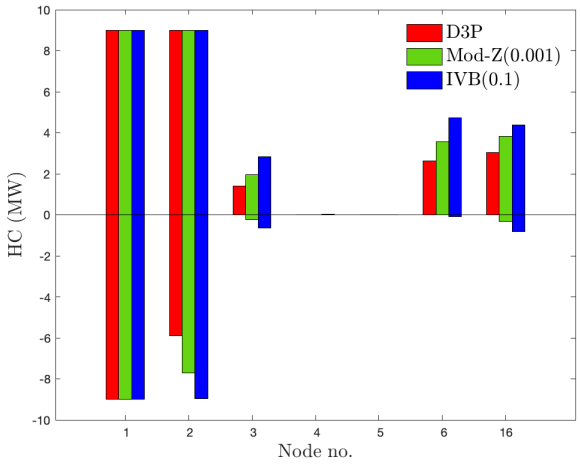

Fig. 7. Comparing the hosting capacity from the IVB(0.1) to that of D3P and Mod-Z. Nodes with zero HC have been excluded in this figure for enhanced clarity.

TABLE III
Comparing the different methods across two networks.

Method	IEEE 37 Node			534-node Feeder		
	HC (MW)	HC (MW)	Run Time (sec)	HC (MW)	HC (MW)	Run Time (sec)
D3P	-14.9	25.1	62	-26.4	46.5	380
IVB(0.1)	-19.5	30.4	314	-59.4	73.0	2973
IVB(1)	-18.2	28.4	79	-59.1	73.0	996
Mod-Z(0.001)	-17.3	27.4	60	-74.3	71.8	439
Random Search	-5.9	12.2	343	-32.9	76.5	2346

Figs. 8 and 9 present $|V^{3\phi}|$ for different methods applied to the 534-node network for $\mathbf{P}_{\text{CIA}}^{\phi,-}$ and $\mathbf{P}_{\text{CIA}}^{\phi,+}$. It can be seen that using the proposed IVB and Mod-Z methods, the voltage margin is smaller, which allows for higher HC as evident in Table III. In Figure 9, the voltages cannot approach the limits due to transformer rating constraints.

It is important to note that the optimization problem may result in very small HC values in some nodes while leading to significantly higher HC values in a few nodes within the system. This discrepancy can raise concerns regarding fairness since only certain consumers will be permitted to install DERs. We consider two sets of w_i, in the objective function and evaluate the HC for a realistic 534-node network under two scenarios using IVB(0.3): 1) Weight values (w_i) are equal for all nodes. 2) Weight values for leaf nodes are doubled compared to other nodes. Modifying the w_i coefficients enables us to expand the locations where DERs can be installed. Specifically, the locations with HC larger than 0.5 MW have increased from 8 to 16. However, this adjustment comes at the cost of reduced $\overline{\text{HC}}$, which decreases from 73.0 MW to 71.0 MW, and reduced $\underline{\text{HC}}$, which decreases from 59.4 MW to 53.0 MW. Future research efforts could delve into exploring the trade-off between fairness in DER allocation and its impact on the overall HC of the grid.

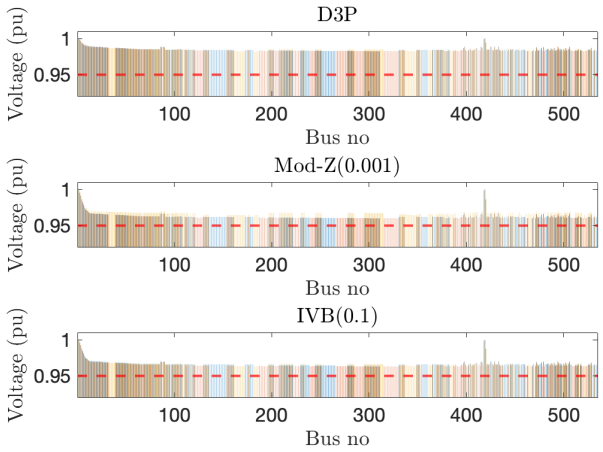

Fig. 8. Voltage profiles for a 534-node feeder are depicted in the figures below for $\mathbf{P}_{\text{CIA}}^{\phi,-}$. In these figures, blue, red, and yellow correspond to phases a, b, and c, respectively.

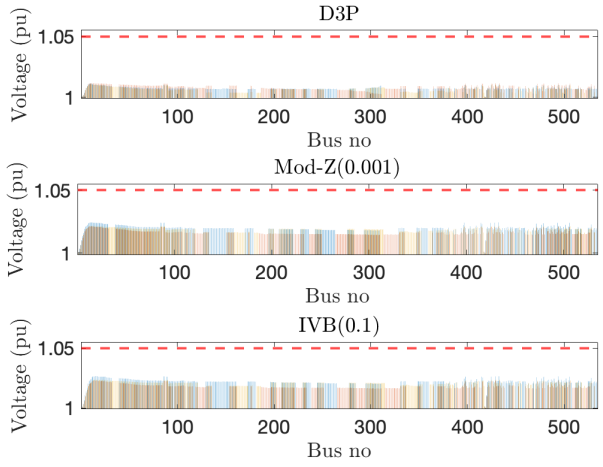

Fig. 9. Voltage profiles for a 534-node feeder are depicted in the figures below for $\mathbf{P}_{\text{CIA}}^{\phi,+}$. In these figures, blue, red, and yellow correspond to phases a, b, and c, respectively.

VI. Conclusion

This paper has introduced a comprehensive approach to obtaining the DER HC in a 3-phase distribution feeder. Leveraging CIA of the AC power flow, our methodology establishes bounds on positive and negative DER injections at each node. Analysis is presented to determine conditions under which this per-phase approach can provide feasible solutions, which comply with 3-phase grid constraints. Furthermore, we have presented an iterative approach to enhance HC by adjusting per-phase voltage bounds. A simulation-based analysis using both the IEEE 37-node test feeder and a real 534-node unbalanced radial distribution feeder is performed and results demonstrate that the proposed iterative method increases the feeder HC. Potential future research directions will consider CIA for full 3-phase networks, as well as comparing its (inherent) conservativeness to the methods presented herein. Additionally, extending the HC analysis methods to meshed distribution and sub-transmission networks will be explored in future work to support interconnection studies.

Acknowledgments

The authors appreciate Nawaf Nazir for his insightful discussions and support throughout the research.

Appendix

A. Derivation of current proxy bounds l^- and l^+

The goal of this appendix is to clarify the structure of the affine $f_{\text{aff}}(.)$ and quadratic $f_{\text{quad}}(.)$ functions that underpin bounds l^-, l^+ used in (9) to engender a convex envelope of l. To derive the lower and upper bounds of l, we consider the second-order Taylor-series approximation of (1d) about an appropriate nominal operating point, $x_{ij}^0 := \text{col}\{P_{ij}^0, Q_{ij}^0, v_j^0\} \in \mathbb{R}^3$. This yields an approximation that is accurate across a range of operating conditions [10]:

$$l_{ij}(P_{ij}, Q_{ij}, V_i) \approx l_{ij}^0(x_{ij}^0) + J_{ij}^\top \delta_{ij} + \frac{1}{2}\delta_{ij}^\top H_{e,ij}\delta_{ij}, \quad (21)$$

where $\delta_{ij} := [P_{ij} - P_{ij}^0, Q_{ij} - Q_{ij}^0, v_j - v_j^0]$, the Jacobian, J_{ij}, and Hessian, $H_{e,ij}$, are defined as

$$J_{ij} := \begin{bmatrix} \frac{2P_{ij}^0}{v_i^0} & \frac{2Q_{ij}^0}{v_i^0} & -\frac{(P_{ij}^0)^2+(Q_{ij}^0)^2}{(v_i^0)^2} \end{bmatrix}, \quad (22)$$

$$H_{e,ij} := \begin{bmatrix} \frac{2}{v_i^0} & 0 & \frac{-2P_{ij}^0}{(v_i^0)^2} \\ 0 & \frac{2}{v_i^0} & \frac{-2Q_{ij}^0}{(v_i^0)^2} \\ \frac{-2P_{ij}^0}{(v_i^0)^2} & \frac{-2Q_{ij}^0}{(v_i^0)^2} & 2\frac{(P_{ij}^0)^2+(Q_{ij}^0)^2}{(v_i^0)^3} \end{bmatrix}. \quad (23)$$

From (21), the square of current magnitude is always positive, so:

$$l_{ij} = |l_{ij}| \approx \left| l_{ij}^0 + J_{ij}^\top \delta_{ij} + \frac{1}{2}\delta_{ij}^\top H_{e,ij}\delta_{ij} \right|. \quad (24)$$

Applying the triangle inequality and the fact that Hessian in (23) is positive semi-definite (PSD) [9], we have

$$l_{ij} \le l_{ij}^0 + \left| J_{ij}^\top \delta_{ij} \right| + \frac{1}{2}\delta_{ij}^\top H_{e,ij}\delta_{ij}. \quad (25)$$

Applying the properties of the maximum operator, we get the quadratic function:

$$l_{ij} \le l_{ij}^0 + \max\left\{ 2\left| J_{ij}^\top \delta_{ij} \right|, \delta_{ij}^\top H_{e,ij}\delta_{ij} \right\}. \quad (26)$$

Note that the RHS of (26) is quadratic in terms of the three physical variables (P_{ij}, Q_{ij}, V_i) that embody δ_{ij}. To characterize the upper bound in terms of the proxy variables requires considering worst-case combinations of upper $(^+)$ and lower $(^-)$ proxy variables, i.e., over all eight combinations: $\delta_{ij}^+ := \delta_{ij}(P_{ij}^+, Q_{ij}^+, V_i^+)$, $\delta_{ij}(P_{ij}^+, Q_{ij}^+, V_i^-)$, …, $\delta_{ij}(P_{ij}^-, Q_{ij}^-, V_i^+)$, and $\delta_{ij}^- := \delta_{ij}(P_{ij}^-, Q_{ij}^-, V_i^-)$. Thus, we get:

$$f_{\text{quad}}(.) := l_{ij}^0 + \max\left\{ 2\left| J_{ij,+}^\top \delta_{ij}^+ + J_{ij,-}^\top \delta_{ij}^- \right|, \psi_{ij} \right\}, \quad (27)$$

where $J_{ij,+}$ and $J_{ij,-}$ are composed of the positive and negative entries of J_{ij}, respecitively, and $J_{ij} = J_{ij,+} + J_{ij,-}$.

Further, $\psi_{ij} := \max\{\delta_{ij}^{+/-} H_{\mathrm{e},ij} \delta_{ij}^{+/-}\}$ is the largest product among the eight proxy pairs. Clearly, relaxing $f_{\text{quad}}(.)$ provides a convex upper bound on l_{ij} as utilized in (9).

For the lower bound, consider (21) and drop the term with PSD $H_{\mathrm{e},ij}$, which gives

$$l_{ij} \geq l_{ij}^0 + J_{ij}^\top \delta_{ij} := \underline{l}_{ij}. \tag{28}$$

Thus, in terms of proxy variables, we get

$$f_{\text{aff}}(.) := l_{ij}^0 + J_{ij,+}^\top \delta_{ij}^- + J_{ij,-}^\top \delta_{ij}^+. \tag{29}$$

This completes the derivations. For full details on these bounds and the CIA-based methods and results (for balanced feeders), please see [9], [10].

REFERENCES

[1] K. Schmitt, R. Bhatta, M. Chamana, M. Murshed, I. Osman, S. Bayne, and L. Canha, "A review on active customers participation in smart grids," *Journal of Modern Power Systems and Clean Energy*, vol. 11, no. 1, pp. 3–16, 2023.

[2] M. Almassalkhi, S. Brahma, N. Nazir, H. Ossareh, P. Racherla, S. Kundu, S. P. Nandanoori, T. Ramachandran, A. Singhal, D. Gayme, C. Ji, E. Mallada, Y. Shen, P. You, and D. Anand, "Hierarchical, grid-aware, and economically optimal coordination of distributed energy resources in realistic distribution systems," *Energies*, vol. 13, no. 23, 2020. [Online]. Available: https://www.mdpi.com/1996-1073/13/23/6399

[3] AusNet Services. (2017) . export limits for embedded generators up to 200 kva connected at low voltage. [Online]. Available: https://www.ausnetservices.com.au/

[4] M. Z. Liu, L. F. Ochoa, P. K. C. Wong, and J. Theunissen, "Using opf-based operating envelopes to facilitate residential der services," *IEEE Transactions on Smart Grid*, vol. 13, no. 6, pp. 4494–4504, 2022.

[5] X. Chen, E. Dall'Anese, C. Zhao, and N. Li, "Aggregate power flexibility in unbalanced distribution systems," *IEEE Transactions on Smart Grid*, vol. 11, no. 1, pp. 258–269, 2020.

[6] E. Dall'Anese, S. S. Guggilam, A. Simonetto, Y. C. Chen, and S. V. Dhople, "Optimal regulation of virtual power plants," *IEEE Transactions on Power Systems*, vol. 33, no. 2, pp. 1868–1881, 2018.

[7] Z. Yuan and M. Reza Hesamzadeh, "A distributed economic dispatch mechanism to implement distribution locational marginal pricing," in *2018 Power Systems Computation Conference (PSCC)*, 2018, pp. 1–7.

[8] S. Ross and J. Mathieu, "Strategies for network-safe load control with a third-party aggregator and a distribution operator," *IEEE Transactions on Power Systems*, vol. 36, no. 4, pp. 3329–3339, 2021.

[9] N. M. Nazir and M. Almassalkhi, "Voltage positioning using co-optimization of controllable grid assets in radial networks," *IEEE Transactions on Power Systems*, vol. 36, no. 4, pp. 2761–2770, 2021.

[10] N. Nazir and M. Almassalkhi, "Grid-aware aggregation and realtime disaggregation of distributed energy resources in radial networks," *IEEE Transactions on Power Systems*, vol. 37, no. 3, pp. 1706–1717, 2022.

[11] D. Lee, K. Turitsyn, D. K. Molzahn, and L. A. Roald, "Feasible path identification in optimal power flow with sequential convex restriction," *IEEE Transactions on Power Systems*, vol. 35, no. 5, pp. 3648–3659, 2020.

[12] D. Lee, K. Turitsyn, D. K. Molzahn, and L. Roald, "Robust AC optimal power flow with robust convex restriction," *IEEE Transactions on Power Systems*, vol. 36, no. 6, pp. 4953–4966, 2021.

[13] V. Bassi, D. Jaglal, L. Ochoa, T. Alpcan, and C. Leckie, "Deliverables 1-2-3a model-free voltage calculations and operating envelopes," University of Melbourne, Technical Report, 7 2022.

[14] K. Petrou, A. T. Procopiou, L. Gutierrez-Lagos, M. Z. Liu, L. F. Ochoa, T. Langstaff, and J. M. Theunissen, "Ensuring distribution network integrity using dynamic operating limits for prosumers," *IEEE Transactions on Smart Grid*, vol. 12, no. 5, pp. 3877–3888, 2021.

[15] V. Rigoni, D. Flynn, and A. Keane, "Coordinating demand response aggregation with lv network operational constraints," *IEEE Transactions on Power Systems*, vol. 36, no. 2, pp. 979–990, 2021.

[16] M. Baran and F. Wu, "Optimal capacitor placement on radial distribution systems," *IEEE Transactions on Power Delivery*, vol. 4, no. 1, pp. 725–734, Jan. 1989. [Online]. Available: http://ieeexplore.ieee.org/document/19265/

[17] R. Heidari, M. M. Seron, and J. H. Braslavsky, "Non-local approximation of power flow equations with guaranteed error bounds," in *2017 Australian and New Zealand Control Conference (ANZCC)*, 2017, pp. 83–88.

[18] K. P. Schneider, B. A. Mather, B. C. Pal, C.-W. Ten, G. J. Shirek, H. Zhu, J. C. Fuller, J. L. R. Pereira, L. F. Ochoa, L. R. de Araujo, R. C. Dugan, S. Matthias, S. Paudyal, T. E. McDermott, and W. Kersting, "Analytic Considerations and Design Basis for the IEEE Distribution Test Feeders," *IEEE Transactions on Power Systems*, vol. 33, no. 3, pp. 3181–3188, 2018.

[19] M.-S. Chen and W. Dillon, "Power system modeling," *Proceedings of the IEEE*, vol. 62, no. 7, pp. 901–915, 1974.

[20] A. Garces. (2023) Linear load flow in power distribution systems: Unbalanced case. Online. MATLAB Central File Exchange. Retrieved September 23, 2023. [Online]. Available: https://www.mathworks.com/matlabcentral/fileexchange/56074-linear-load-flow-in-power-distribution-systems-unbalanced-case